

AD-A011 586

SINGER: A COMPUTER CODE FOR GENERAL ANALYSIS OF  
TWO-DIMENSIONAL CONCRETE STRUCTURES. VOLUME 4.  
DEMONSTRATION PROBLEMS

R. M. Barker, et al

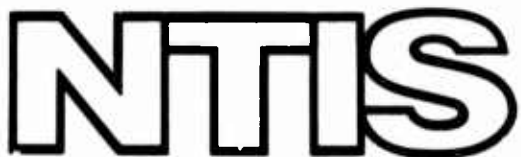
Virginia Polytechnic Institute and State University

Prepared for:

Air Force Weapons Laboratory  
Defense Nuclear Agency

May 1975

DISTRIBUTED BY:



National Technical Information Service  
U. S. DEPARTMENT OF COMMERCE

ADA011586

AFWL-TR-74-228, Vol. IV

AFWL-TR-  
74-228  
Vol. IV

191135

# SINGER: A COMPUTER CODE FOR GENERAL ANALYSIS OF TWO-DIMENSIONAL CONCRETE STRUCTURES

Volume IV

Demonstration Problems

R. M. Barker

R. J. Melosh

S. M. Holzer

J. C. Bradshaw

May 1975

Final Report for Period August 1972 - August 1974



Vol IV  
191135

Approved for public release; distribution unlimited.

Prepared By

DEPARTMENT OF CIVIL ENGINEERING

Virginia Polytechnic Institute and State University

Blacksburg, Virginia

AIR FORCE WEAPONS LABORATORY

Air Force Systems Command

Kirtland Air Force Base, NM 87117

Reproduced by  
NATIONAL TECHNICAL  
INFORMATION SERVICE  
U S Department of Commerce  
Springfield VA 22151

This final report was prepared by the Department of Civil Engineering Virginia Polytechnic Institute and State University, Blacksburg, Virginia under Contract F29601-73-C-0022, Program Element 62704H, Project 5710, WDNS 3414, Subtask Y99QAXSC157, with the Air Force Weapons Laboratory, Kirtland Air Force Base, New Mexico. Rodney G. Galloway, 2 LT, USAF, was the Laboratory Project Officer-in-Charge. Major Tyler M. Jackson was the former Laboratory Project Officer.

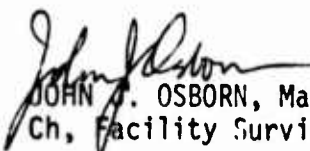
When US Government drawings, specifications, or other data are used for any purpose other than a definitely related government procurement operation, the Government thereby incurs no responsibility nor any obligation whatsoever, and the fact that the Government may have formulated, furnished, or in any way supplied the said drawings, specifications, or other data is not to be regarded by implication or otherwise as in any manner licensing the holder or any other person or corporation or conveying any rights or permission to manufacture, use or sell any patented invention that may in any way be related thereto.

This technical report has been reviewed and is approved for publication.



RODNEY G. GALLOWAY, 2 LT, USAF  
Project Officer

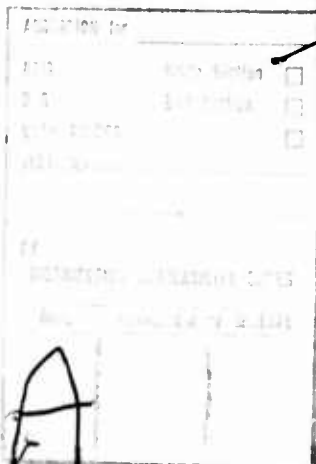
FOR THE COMMANDER



JOHN A. OSBORN, Major, USAF  
Ch, Facility Survivability Branch



W. B. LIDDICOET, Colonel, USAF  
Ch, Civil Engineering Research Division



DO NOT RETURN THIS COPY. RETAIN OR DESTROY.

~~UNCLASSIFIED~~

**SECURITY CLASSIFICATION OF THIS PAGE (When Data Entered)**

**DD FORM 1 JAN 72 1473 EDITION OF 1 NOV 68 IS OBSOLETE**

~~UNCLASSIFIED~~

~~SECURITY CLASSIFICATION OF THIS PAGE (When Data Entered)~~

## CONTENTS

<u>Section</u>		<u>Page</u>
1	INTRODUCTION . . . . .	5
2	DEMONSTRATION PROBLEMS . . . . .	6
2.1	PLASTIC BEAM . . . . .	6
2.2	ELASTIC RING . . . . .	12
2.3	ELASTICA . . . . .	10
2.4	DYNAMIC ROD. . . . .	26
	APPENDIX - INPUT DATA FOR PROBLEMS . . . . .	34

## FIGURES

<u>Figure</u>	<u>Page</u>
2.1    Cantilever Beam with Concentrated Load on Tip. . . . .	8
2.2    Idealized Stress-Strain Curves . . . . .	9
2.3    Inelastic Stress and Curvature Diagrams. . . . .	11
2.4    Comparison of Tip Deflection . . . . .	14
2.5    Elastic Ring Under Internal Pressure . . . . .	15
2.6    Idealization for Elastic Ring. . . . .	17
2.7    Variation of Relative Error with Number of Segments in One-Quarter of an Elastic Ring . . . . .	20
2.8    Thin Elastic Rod Subjected to Large Axial Force and End Moments. . . . .	21
2.9    Nondimensional Comparison of Load and Center Line Deflection. .	23
2.10   Nondimensional Comparison of Load and Longitudinal Deflection .	24
2.11   Dynamic Rod. . . . .	27
2.12   Stress-Strain Curve. . . . .	27
2.13 $i^{\text{th}}$ Response Domain. . . . .	28
2.14   Stress-Strain Response . . . . .	28
2.15   Stress History . . . . .	??
2.16   Stress History of Rod. . . . .	33

TABLES

<u>Table</u>		<u>Page</u>
1	Demonstration Problems.....	7
2	Cantilevered Beam with a Vertical Load on the Free End.....	13
3	Elastic Ring Under Internal Pressure.....	18
4	Deflection Results for the Elastic Problem.....	25
5	A Dynamic Response of Inelastic Rod.....	30

## SECTION 1

### INTRODUCTION

This report describes the problems that have been selected to demonstrate the modeling capabilities of the SINGER computer code. The problems have been chosen to show that the computer code has the ability to predict the large deflection, finite strain, static and dynamic response of two dimensional frames and rings composed of straight line beam-column elements.

The problems have been selected so that each has an independent solution check. This limits the scope of the individual problems (especially when the independent check is a hand calculation) and each problem is able to check only a few features of the program. However, as a group, the problems permit checking all major features of the program and have proven effective in developing a program which can model relatively complex interacting inelastic and nonlinear effects.

The next section briefly describes each of the four problems selected and gives a comparison of the results obtained by SINGER with those obtained by the independent check. The data sets used in executing these problems are given in an appendix to the report.

## SECTION 2

### Demonstration Problems

The four problems selected are: (1) plastic beam, (2) elastic ring, (3) elastica, and (4) dynamic rod. Table 1 indicates the program features tested by each problem and the source of the independent solution checks that will be used to evaluate the accuracy of the SINGER analysis.

#### 2.1 PLASTIC BEAM

The steel wide flange beam of Figure 2.1 is loaded with a concentrated load,  $P$ , in the direction of the  $y$ -axis on the free end. The loading is monotonically increased so that system deformations and strains pass through the elastic range into the inelastic range.

The beam is cantilevered and has a length,  $L$ , of 144 inches. It has a flange width,  $b$ , of 6 inches; flange thickness,  $t_f$ , of 1 inch; web thickness,  $t_w$ , of 1 inch; and a total depth,  $h$ , of 12 inches. This beam was analysed with two different stress-strain curves as shown in Figure 2.2. In each case, the yield point is 33,000 psi, and Young's modulus is 29,000,000 psi.

In the elastic range, vertical tip deflections were calculated according to the relation

$$\Delta_{tip} = \frac{PL^3}{3EI} \quad (2.1)$$

where  $E$  is Young's modulus, and  $I$  is the moment of inertia about the  $z$ -axis which for this beam is 447.33 in.<sup>4</sup>

In the inelastic range, an analytical solution for deflections was made for the elastic-perfectly plastic material (Figure 2.2a) and

TABLE 1  
DEMONSTRATION PROBLEMS

Number	Name	Features Tested	Check
1	Plastic Beam	Nonlinear material model, static analysis equation solution, stress analysis	exact solution
2	Elastic Ring	Coordinate transformations, symmetric displacement constraints, distributed loadings, multidegree of freedom capability	exact solution
3	Elastica	Large deflections, adaptive transformations, geometric modeling tests	numerical solution (Huddleston)
4	Dynamic Rod	Cyclic loading, failure model, dynamic analysis capability, stress modeling limits.	exact solution

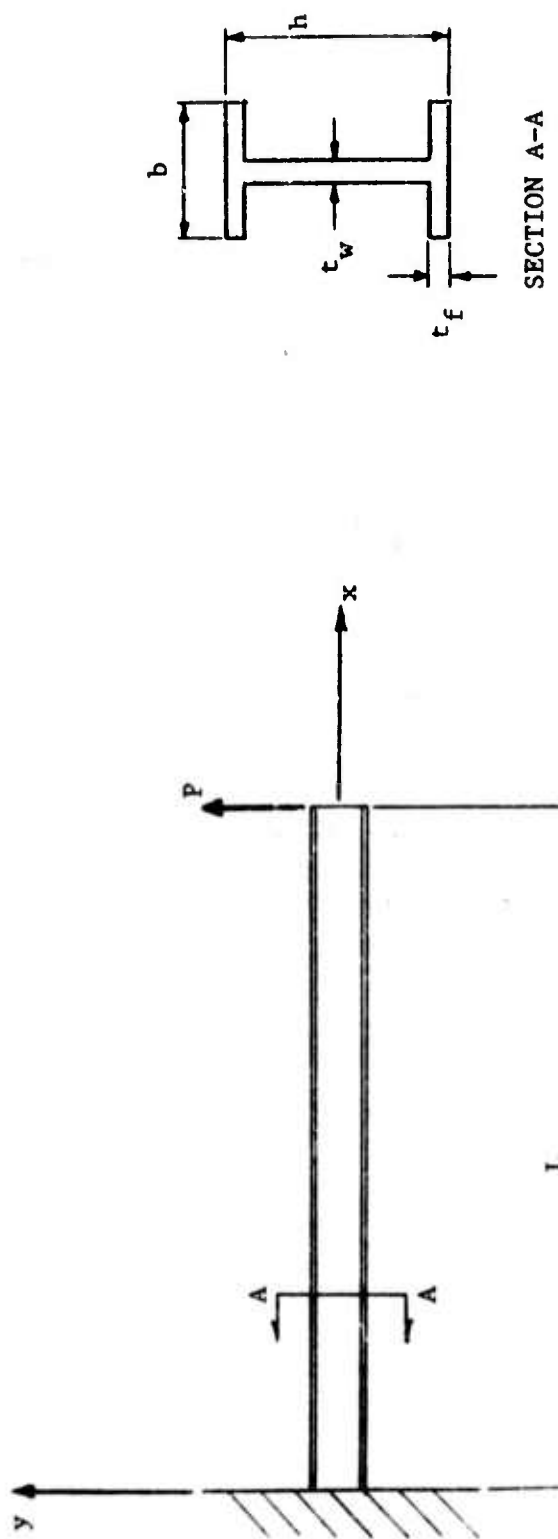
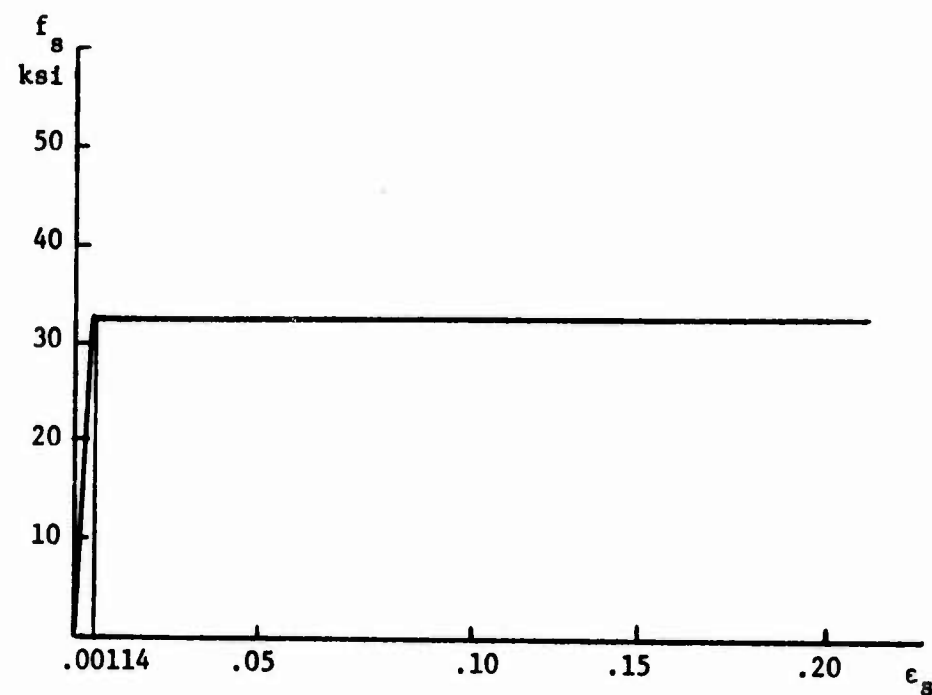
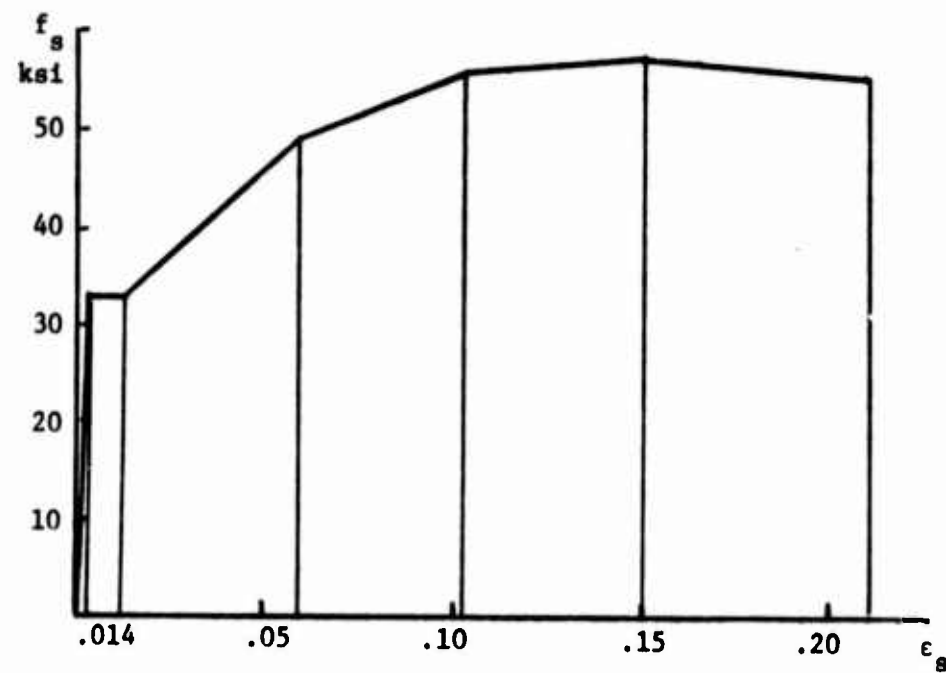


Figure 2.1 - Cantilever Beam with Concentrated Load on Tip.



a) Elastic-Perfectly Plastic.



b) With Strain Hardening.

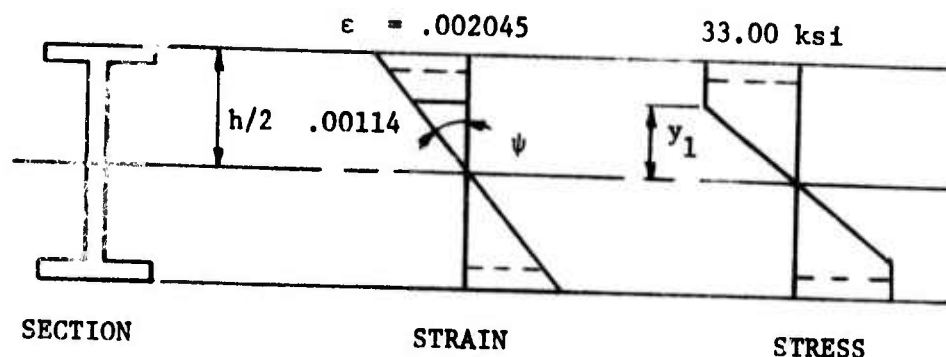
Figure 2.2 - Idealized Stress-Strain Curves.

for the material in which strain hardening was allowed (Figure 2.2b). For a given load, the moment diagram is known. The stress block at the support is determined by equating the integral of the statical moment of the stresses to the applied moment. The height of the elastic portion,  $y_1$ , is then determined and, from similar triangles, the strain at the extreme fiber is found. The curvature,  $\psi$ , is obtained by dividing the extreme fiber strain by the depth of the neutral axis. The tip deflection is, by moment-area principles, equal to the moment of the curvature diagram about the free end of the cantilever. It should be noted that this analysis does not consider the effect of axial deformation.

The yield load was found to be 17,086 lbs, and the collapse load for the elastic-perfectly plastic case was determined as 20,850 lbs. This collapse load was obtained by setting  $y_1$  of Figure 2.3 to zero.

In the analysis with an elastic-perfectly plastic stress-strain curve, the beam was divided into several different elements of varying lengths. Studies of the beam as 1, 2, 3, and 6 elements with three load steps were made. The step loadings were 82%, 99%, and 117% of the yield load.

The results were more accurate in the cases in which the beams were divided so that the energy participation of the elements was evenly distributed. Output from SINGER includes this information on energy participation. Elements with a high percentage of participation are simply subdivided. The 6 element beam gave excellent results, but a 2 element beam with a 114 inch member and a 30 inch member at the support, where yielding began, gave comparable results. In the beams



$P = 20.00 \text{ k}$

$$M_3 = 2880.00 \text{ in-k}$$

$$M_y = 2460.33 \text{ in-k}$$

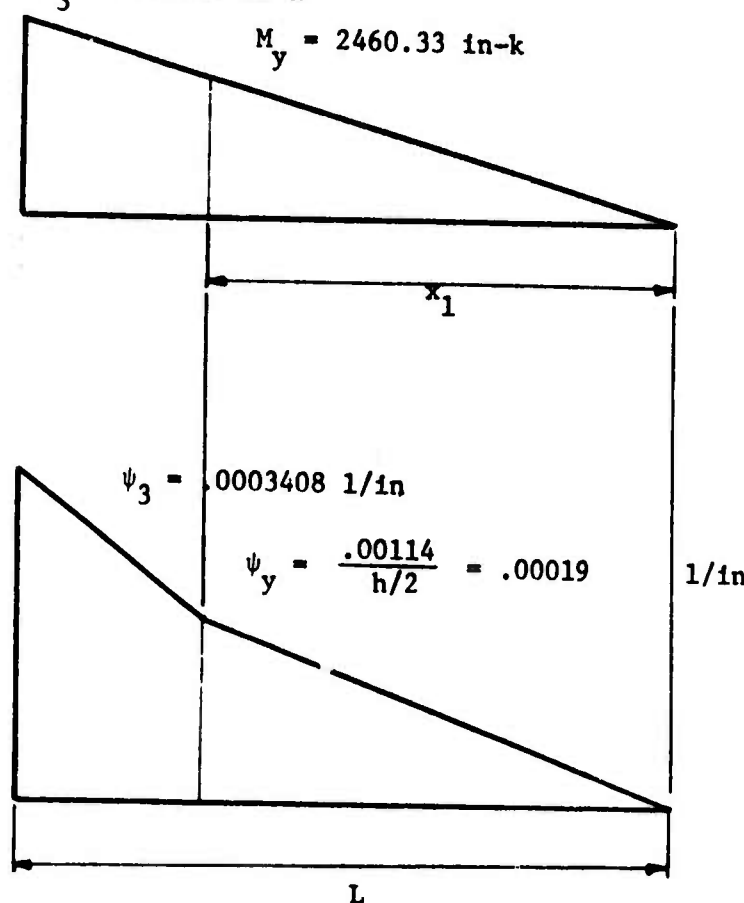


**Figure 2.3 - Inelastic Stress and Curvature Diagrams.**

that the elements were not selected to balance the energy distribution and also the beam considered as one element, it was found that yielding would occur during the 99% load step.

In analysing the beam with strain hardening allowed as shown in Figure 2.2b, eight elements were selected. The elements were arranged with the smaller ones at the support and the longer ones at the free end so that the energy participation of the elements would be balanced. The SINGER results are shown in Table 2 and in Figure 2.4 as load versus deflection with non-dimensional units.

The SINGER results of the inelastic beam were in close agreement with the analytical results, especially if the elements were chosen so that the energy participation was balanced. It was seen that a system of few elements properly chosen will give results comparable to a system with a large number of elements. When strain hardening is allowed, the SINGER results vary from the analytical results as shown in Figure 2.4. The SINGER results differ from the analytical results since the analytical results do not include the effect of axial deformation.

## 2.2 ELASTIC RING

The steel ring of Figure 2.5 is symmetrically loaded by a uniformly distributed internal pressure,  $p$ . The loading is chosen so that system deformations and strains that are within the elastic range and linear analysis assumptions are valid.

The ring has a radius,  $r$ , of 36 inches; thickness,  $t$ , of 2 inches; and a width,  $b$ , of 1 inch. The material is linearly elastic and has a Young's modulus of 29,000,000 psi. The internal pressure is taken as 2000 psi to keep the stresses well within the elastic range.

TABLE 2  
CANTILEVERED BEAM WITH A VERTICAL LOAD ON THE FREE END

$$P_y = 17,086 \text{ lbs} \quad L = 144 \text{ in.}$$

---

Tip Deflection, inches		
$P/P_y$	Analytical*	SINGER
0.82	1.076	1.076
1.00	1.313	1.313
1.22	5.310	3.900
1.67	33.337	32.162
1.94	61.516	48.002
2.07	79.976	54.636

\*neglects effect of axial deformation

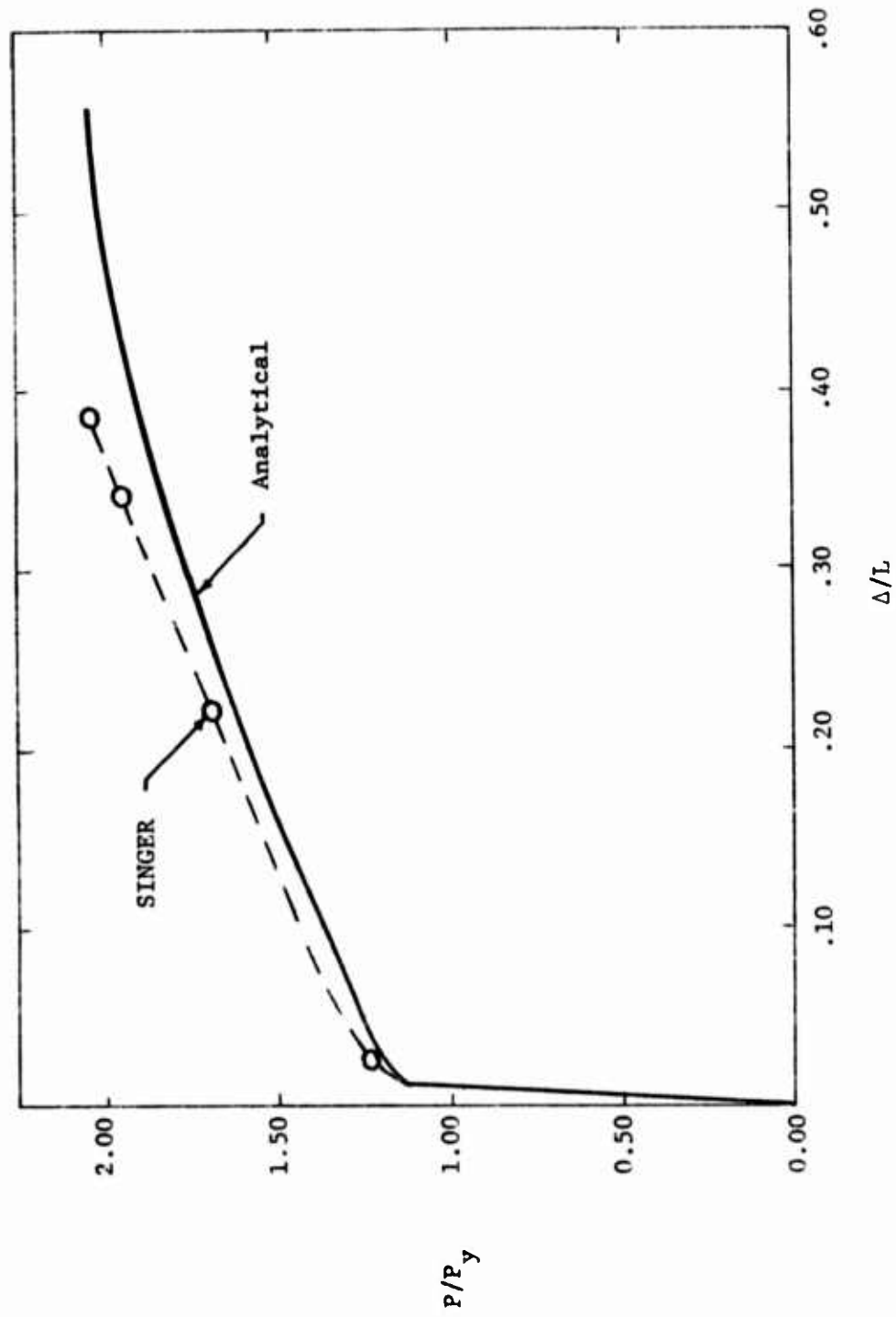


Figure 2.4 - Comparison of Tip Deflection.

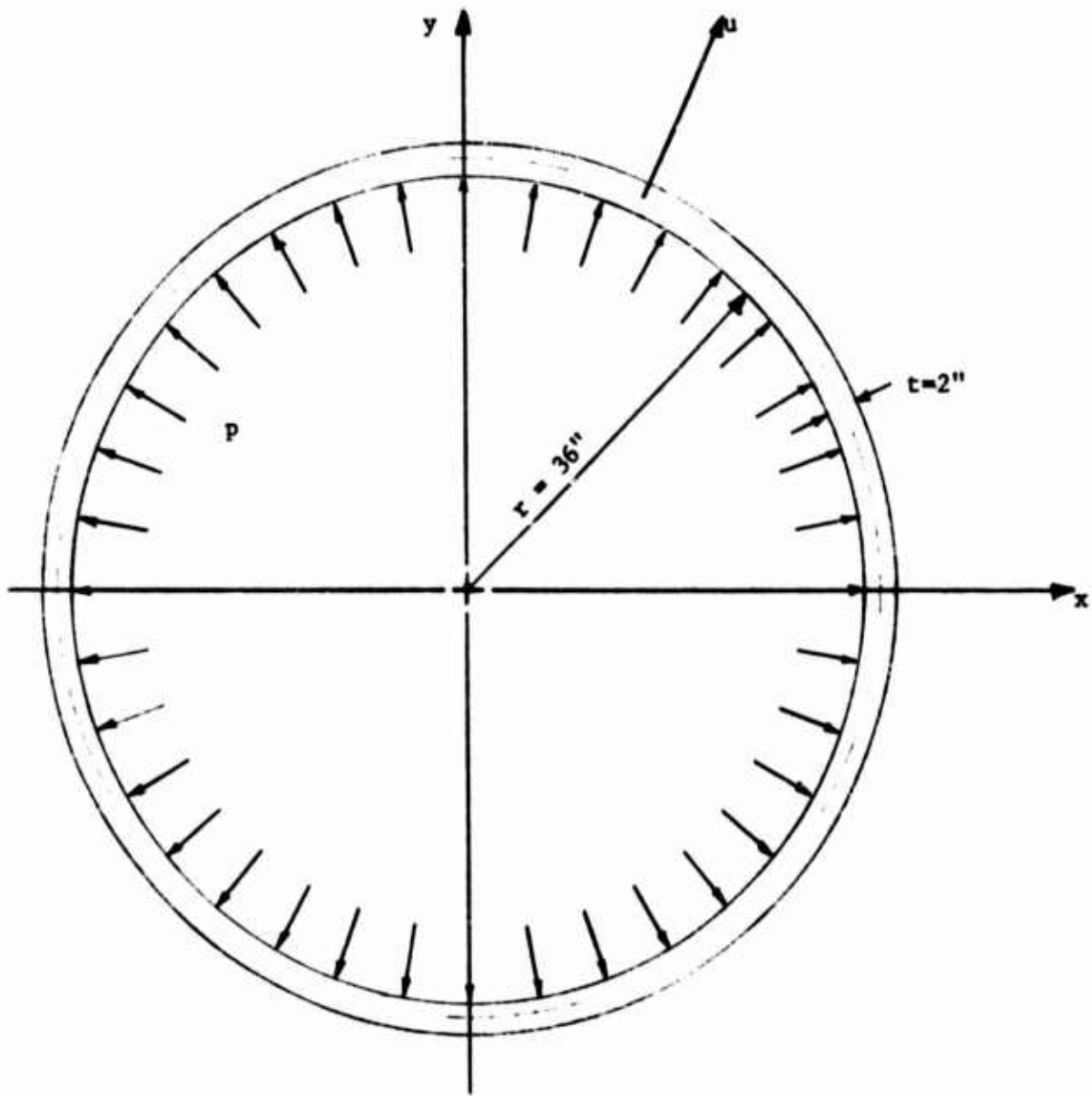


Figure 2.5 - Elastic Ring Under Internal Pressure.

Since the ratio of the ring thickness to its radius is small, uniform normal stresses can be assumed, and thereby no bending moments exist in the ring. Also, because of symmetry in geometry and loading, no shear forces are present. From the well known ring equations, the hoop force is given by

$$T_{\text{exact}} = pr \quad (2.2)$$

and the radial displacement is

$$u_{\text{exact}} = \frac{r^2 p}{Et} \quad (2.3)$$

where E is Young's modulus. For internal pressure of 2000 psi, the hoop force for the example problem is 72,000 pounds and the radial displacement is 0.04469 inch.

In idealizing the ring for SINGER, a number of straight line segments in the first quadrant were used as shown in Figure 2.6. The ring quadrant was restrained from rotation and axial displacement at the boundaries to simulate a complete ring. A uniformly distributed load P of 2000 pounds/inch was imposed normal to the axis of each segment to represent internal pressure.

To determine the number of segments required to adequately represent the ring section, data sets with the quadrant divided into 3, 4, 6, 9, and 18 segments were analysed by SINGER. The same geometric and material properties were used for each data set. The only variation among the data sets was the number of segments.

The results of the analyses are shown in Table 3. The hoop force, T, and the radial displacement, u, were in close agreement with the actual values calculated. Since the ring sections were divided into beam sections, SINGER gave some shear and bending moment at each joint, but these values were negligible (five orders of magnitude smaller than the axial force).

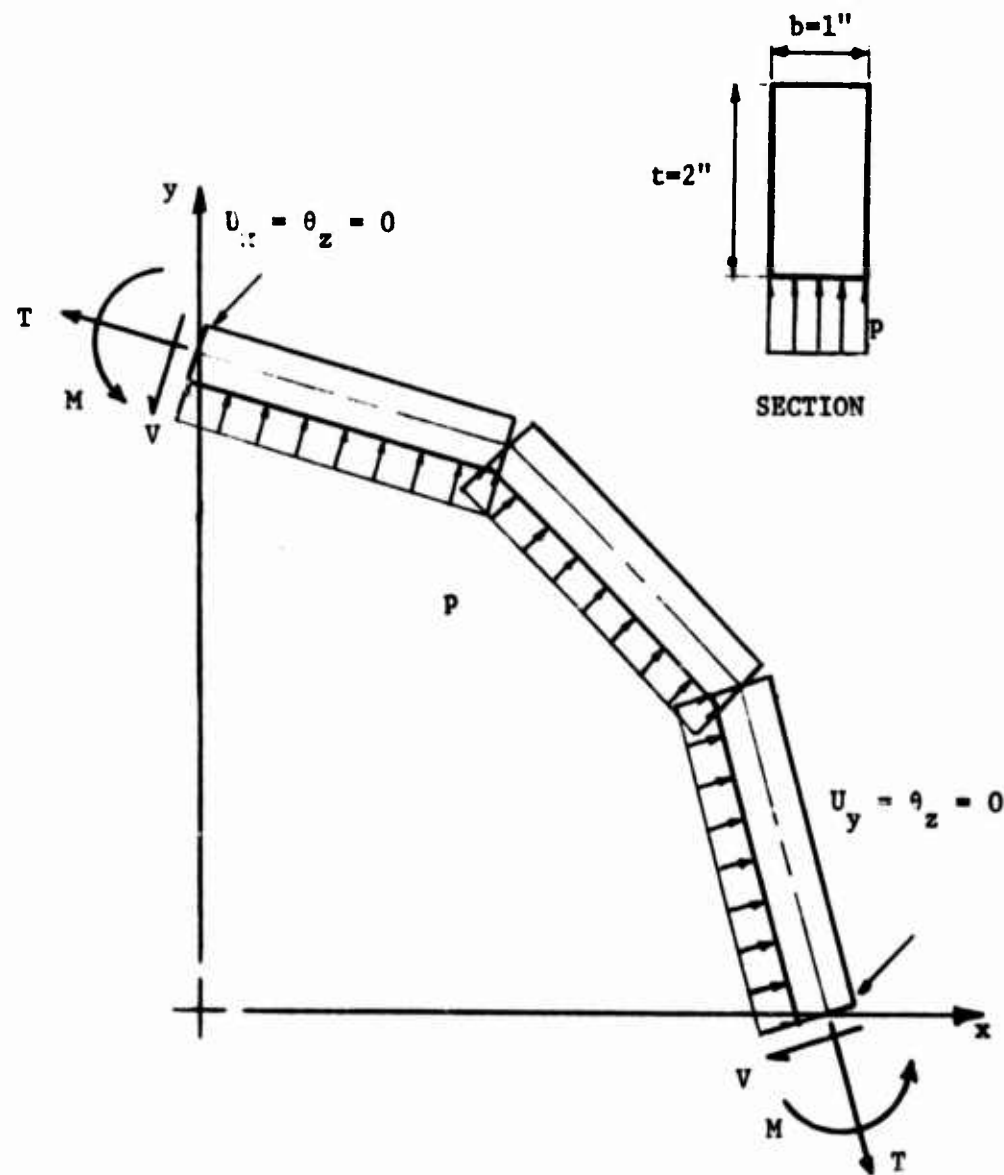


Figure 2.6 - Idealization for Elastic Ring.

TABLE 3  
ELASTIC RING UNDER INTERNAL PRESSURE

$p = 2000 \text{ psi}$        $T_{\text{exact}} = 72,000 \text{ lb}$        $u_{\text{exact}} = 0.04469 \text{ in}$

No. of Segments	$T, \text{lb}$	$u, \text{in.}$	$M_{\text{max}}, \text{in-lb}$	$V_{\text{max}}, \text{lb}$
3	69,547	.0413	.45664	.02269
4	70,616	.04383	-.34581	.01808
6	71,384	.04431	.35453	-.04174
9	71,726	.04452	.41387	-.04453
18	71,932	.04465	.82220	.18102

The accuracy of the SINGER results as compared with the actual calculations is shown in Figure 2.7. In the figure,  $F$  and  $F_{\text{exact}}$  can be either  $T$  and  $T_{\text{exact}}$  or  $u$  and  $u_{\text{exact}}$ .

Since the results for all the data sets have a relative error of less than 3.5%, it can be stated that SINGER models coordinate transformations, displacement constraints, and distributed loadings well. The analysis of the 18 segment ring section shows that SINGER can also handle multi-degree of freedom systems. It can be concluded that for analyzing rings, it is sufficient to model a quadrant with 9 straight line segments. It can be seen in Figure 2.7 that this gives results comparable to those with twice as many segments and with considerably less input and computing effort.

### 2.3 ELASTICA

The simply supported rod of Figure 2.8 is subjected to the slowly applied axial load,  $P$ , and end moments,  $M$ . The load is increased so that large deflections occur. Since the load is near the Euler buckling load, the beam-column will have nonlinear geometrical behavior.

The rod in Figure 2.8 has a length,  $L$ , of 15 feet and cross sectional dimensions of 0.2 inches by 0.2 inches. The Young's modulus for the material is 29,000,000 psi, and there is no yield stress so that the material is perfectly elastic.

The "elastica" problem was proposed by Euler in 1744. A closed form solution for this problem cannot be obtained, but Huddleston<sup>1</sup> provides an independent numerical solution. The classical approach to solving the "elastica" problem is to solve a nonlinear differential equation in terms

---

<sup>1</sup>Huddleston, J. V., "A Numerical Technique for Elastica Problems." Journ. Struct. Div. ASCE, Vol. EM5, Oct. 1968, pp. 1159-1165.

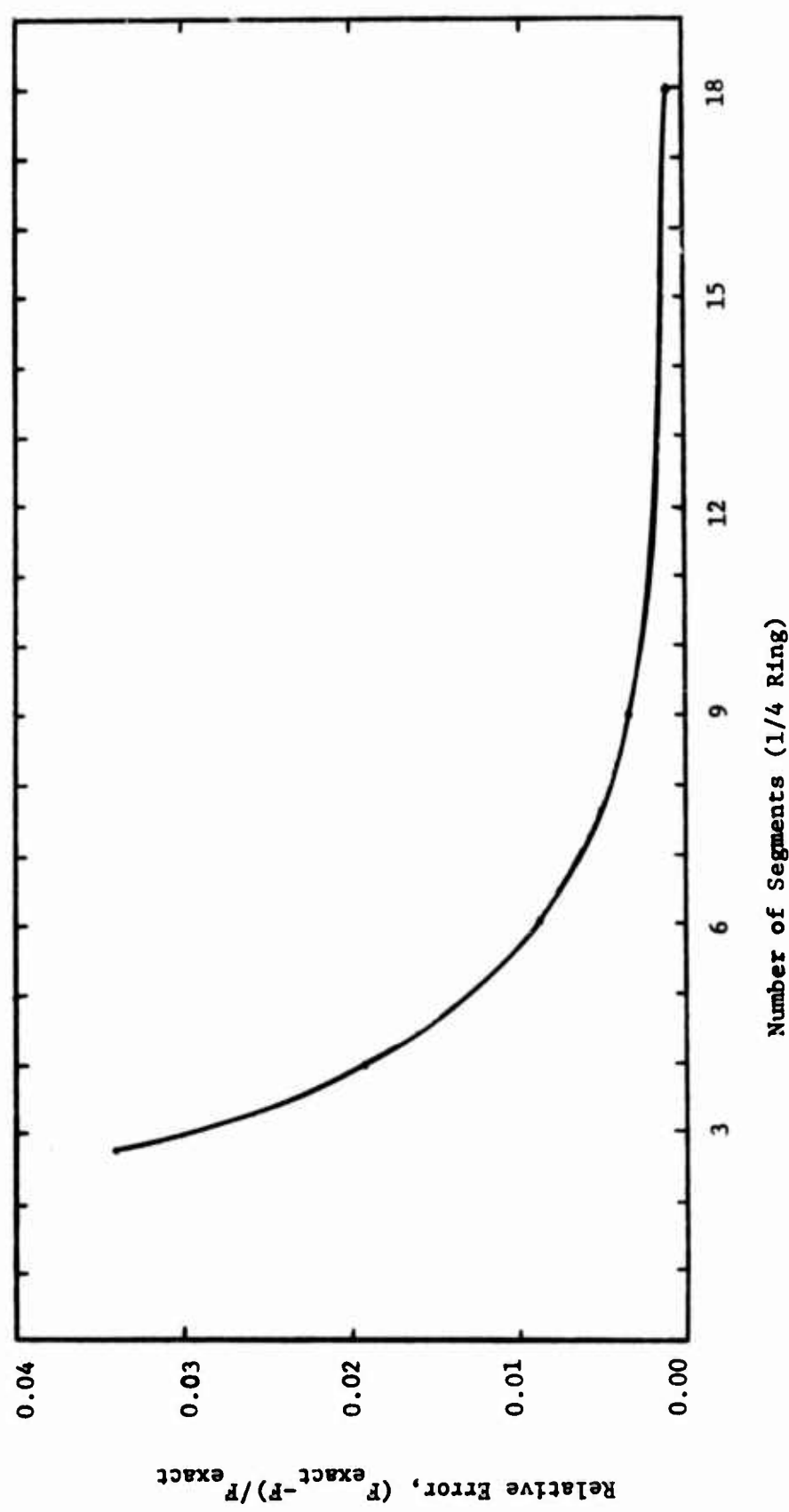


Figure 2.7 - Variation of Relative Error with Number of Segments in One-Quarter of an Elastic Ring.

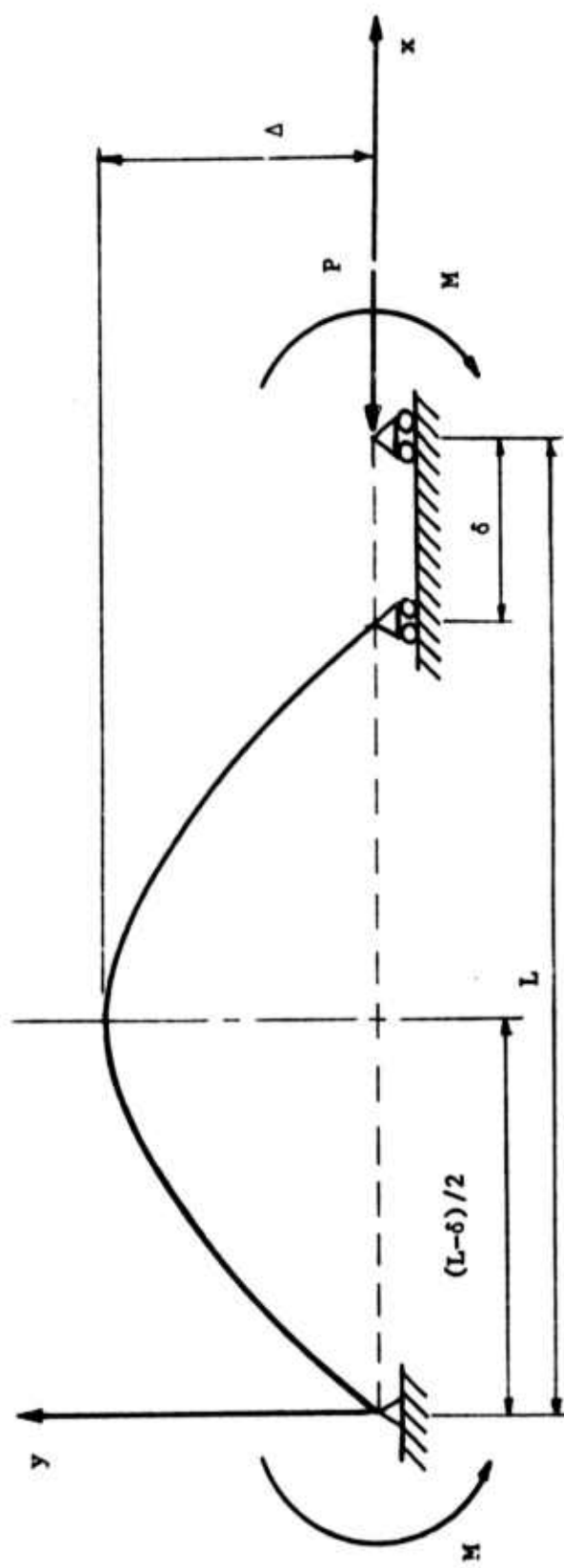


Figure 2.8 - Thin Elastic Rod Subjected to Large Axial Force and End Moments

of elliptic integrals. Huddleston uses a numerical method in solving the nonlinear boundary-value problem. In particular, he employs a "shooting" method, where initial conditions are assumed, integration is performed by a predictor-corrector method, and terminal conditions are computed. An iterative process is used to adjust the initial conditions until the boundary conditions are satisfied.

Figure 2.9 shows the results of Huddleston's solution for a thin rod loaded with an eccentricity,  $e/L$ , of 0.01. Dimensionless load is plotted against dimensionless deflection of the center line. To non-dimensionalize the load, the Euler buckling load,  $P_E$ , was used. The longitudinal deflection at the roller versus the axial load is shown in Figure 2.10.

The SINGER analysis results were also non-dimensionalized. The loading was stepped in 1% increments of the Euler buckling load reaching a maximum of 94%. These results for center line deflection and longitudinal deflection are shown in Figures 2.9 and 2.10 and in Table 4.

In performing the SINGER analysis, examples with the rod divided into different numbers of elements were studied. It was found that the best results were obtained from the examples which contained a large number of elements, in particular, those with 30 elements. The results were better in the examples where the elements were smaller at the center of the rod and larger on the ends of the rod. This variation in element lengths distributed the energy participation more evenly than in the examples with equal element lengths.

The comparison of the Huddleston and SINGER results in Table 4 shows that SINGER is capable of handling large deflections. It can be concluded that the SINGER code can simulate systems whose equilibrium position depends on adequate representation of geometric non-linearities.

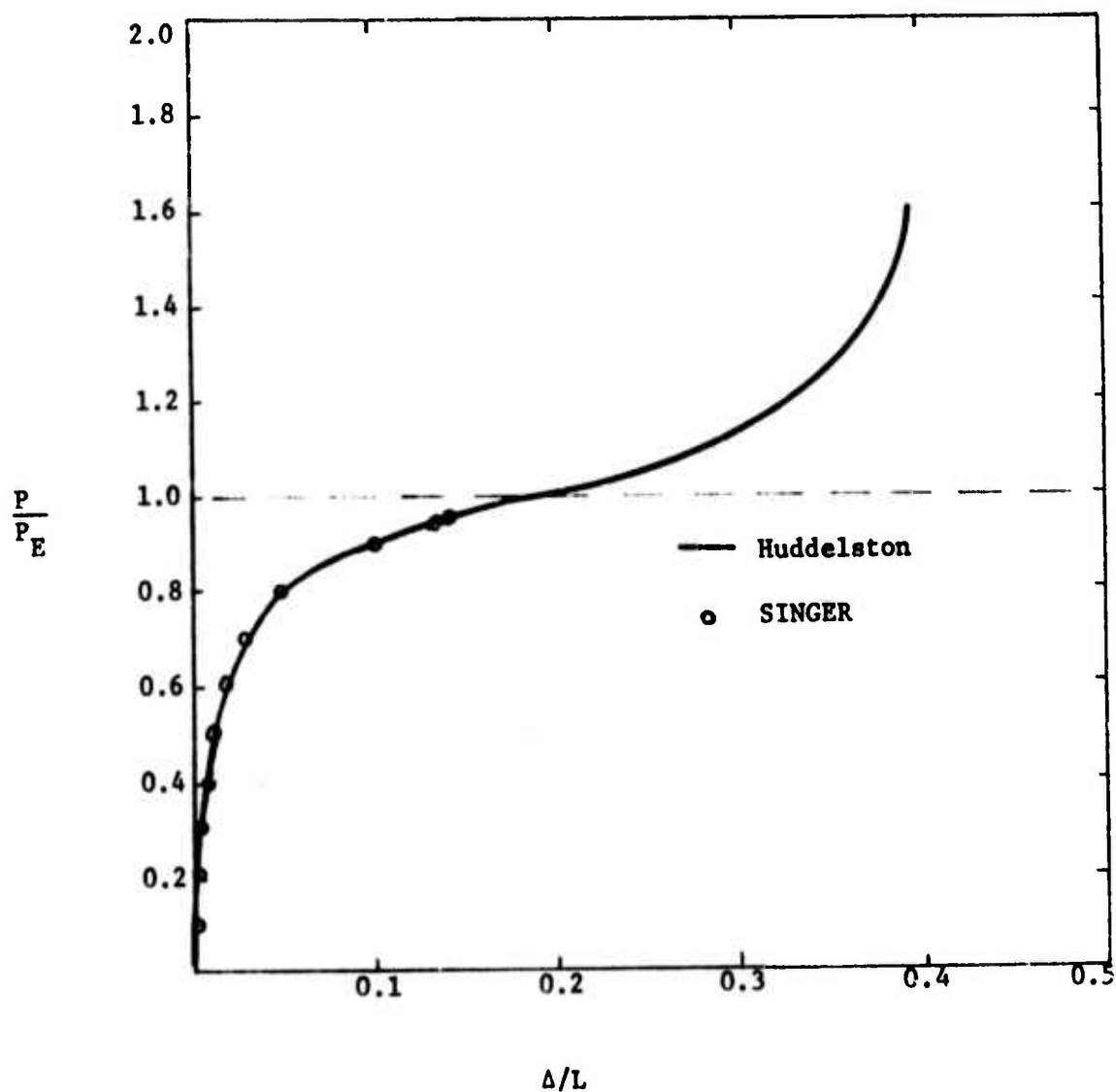


Figure 2.9 - Non-Dimensional Comparison of Load and Center Line Deflection.

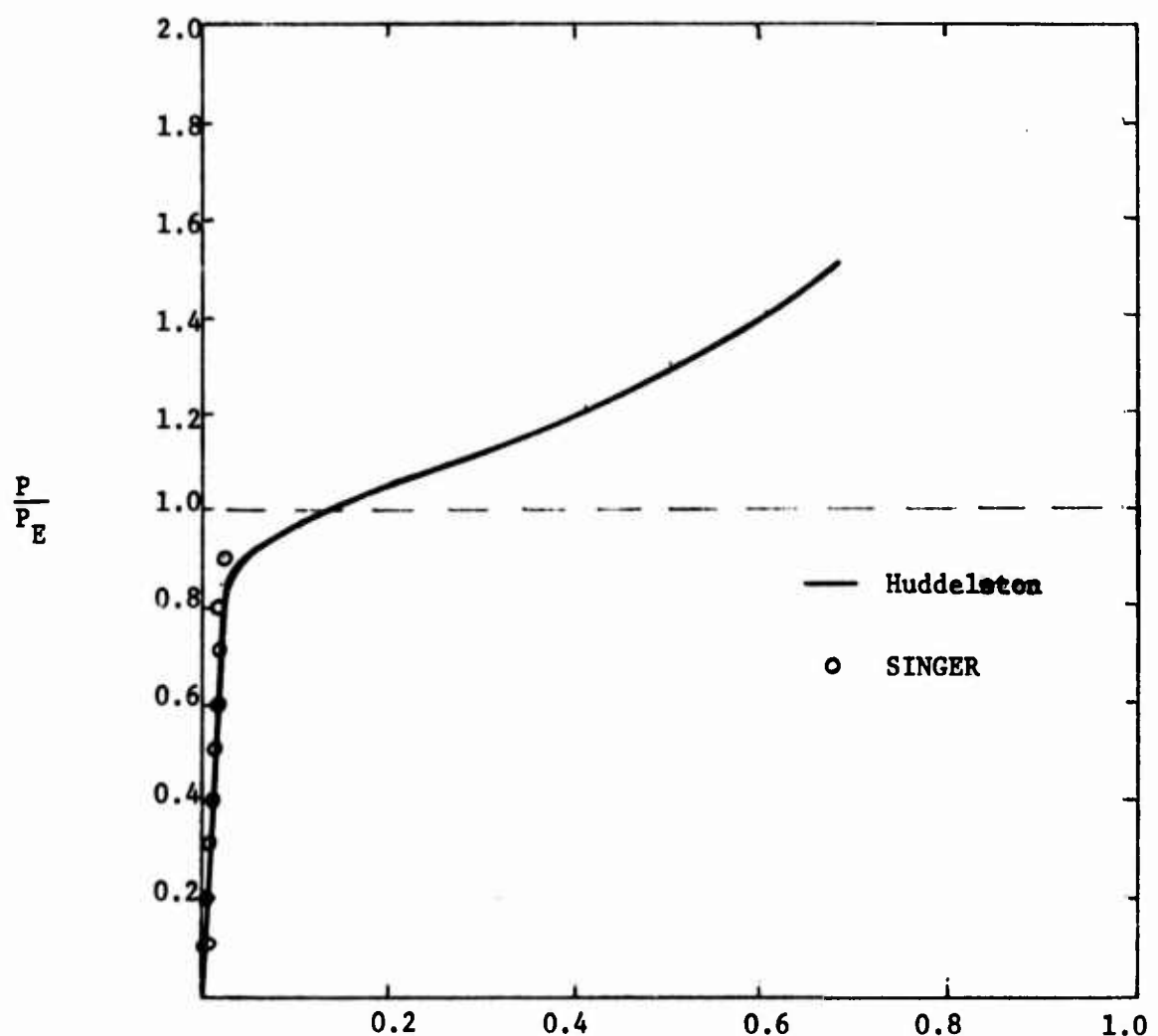


Figure 2.10 - Non-Dimensional Comparison of Load and Longitudinal Deflection.

TABLE 4  
DEFLECTION RESULTS FOR THE ELASTICA PROBLEM

UNITS: INCHES

$P/P_E$	Center-line Deflection		Longitudinal Deflection	
	SINGER	Huddleston	SINGER	Huddleston
0.1	0.25	0.27	0.01	0.18
0.2	0.56	0.63	0.01	0.54
0.3	0.96	0.90	0.01	0.90
0.4	1.50	1.26	0.03	1.26
0.5	2.25	2.16	0.07	1.44
0.6	3.39	3.33	0.16	1.62
0.7	5.27	5.40	0.39	1.80
0.8	8.96	9.00	1.12	3.60
0.9	18.17	18.00	4.64	7.20

## 2.4 DYNAMIC ROD

Figure 2.11 depicts a uniform mass-less rod attached to a support with a concentrated mass at the free end. The constitutive law of the material is defined in Figure 2.12. At time zero, the unstrained state of the rod ( $x=0$ ) is excited by an impulse, which is large enough to induce inelastic deformations but does not cause fracture. Consequently, the rod undergoes cyclic motion, dissipates energy during inelastic response, and attains harmonic motion as a limit state.

The purpose of this problem is to demonstrate the ability of SINGER to predict inelastic cyclic response of systems. Since the response of the rod to an initial impulse can be expressed in explicit form, it serves as a basis for assessing the quality of the response predictions produced by SINGER.

The internal force-displacement relation of the rod is piecewise linear. The corresponding displacement functions can be described by two general expressions. If the stiffness of the rod is nonzero during the  $i^{\text{th}}$  linear internal force-displacement domain (Figure 2.13), the displacement function assumes the form

$$x(\tau) = -d_i + (x_i + d_i) \cos \omega_i \tau + \frac{v_i}{\omega_i} \sin \omega_i \tau, \quad (2.4)$$

where

$$d_i = \frac{r_i}{k_i} - x_i, \quad (2.5)$$

$$k_i = \frac{AE_i}{l}, \quad (2.6)$$

$$\omega_i = \sqrt{k_i/m}, \quad (2.7)$$

$$\tau = t - t_i, \quad (2.8)$$

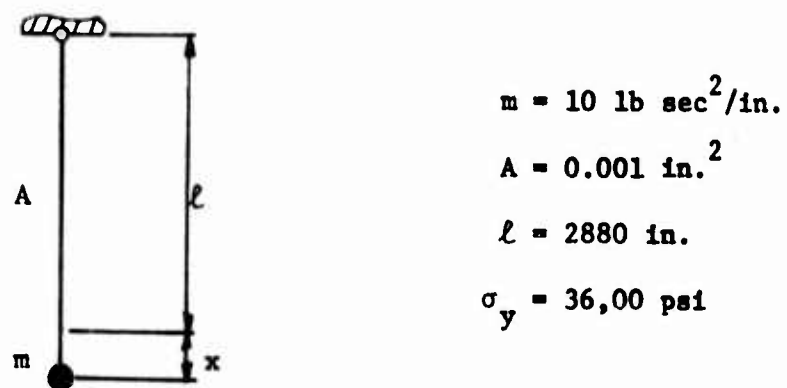


Figure 2.11. Dynamic Rod

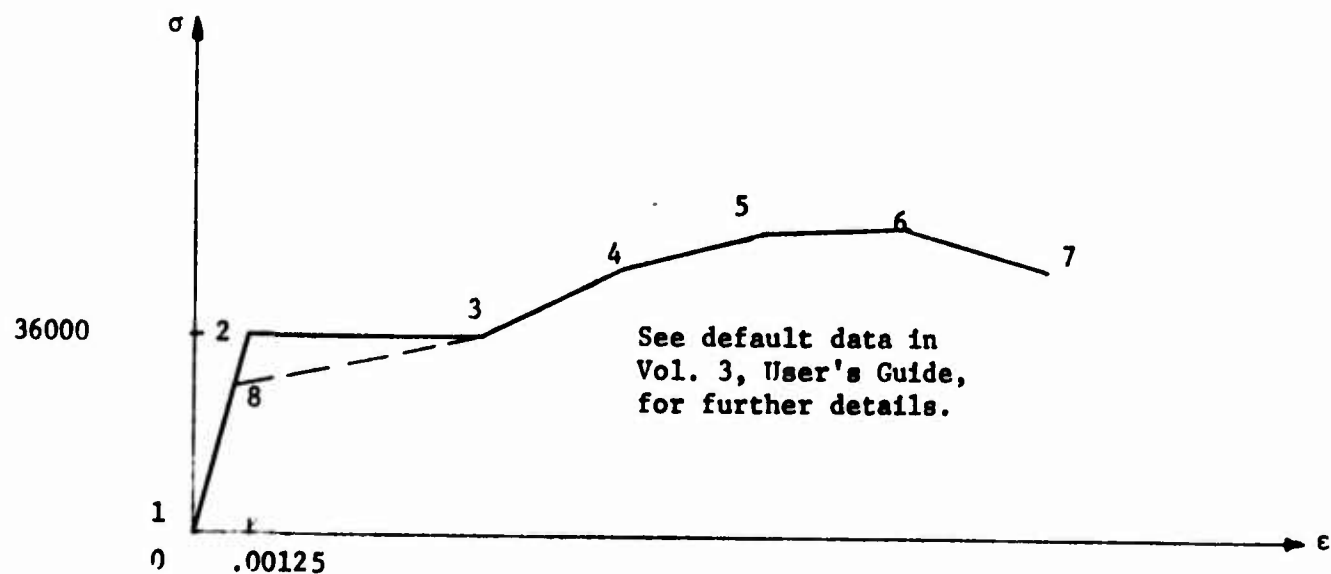


Figure 2.12. Stress-Strain Curve

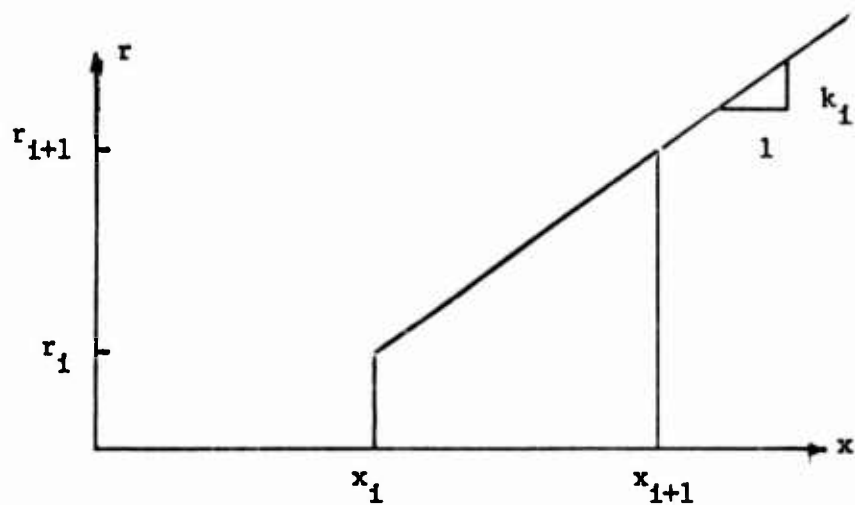


Figure 2.13.  $i^{\text{th}}$  Response Domain  
 $(x_i \leq x \leq x_{i+1})$

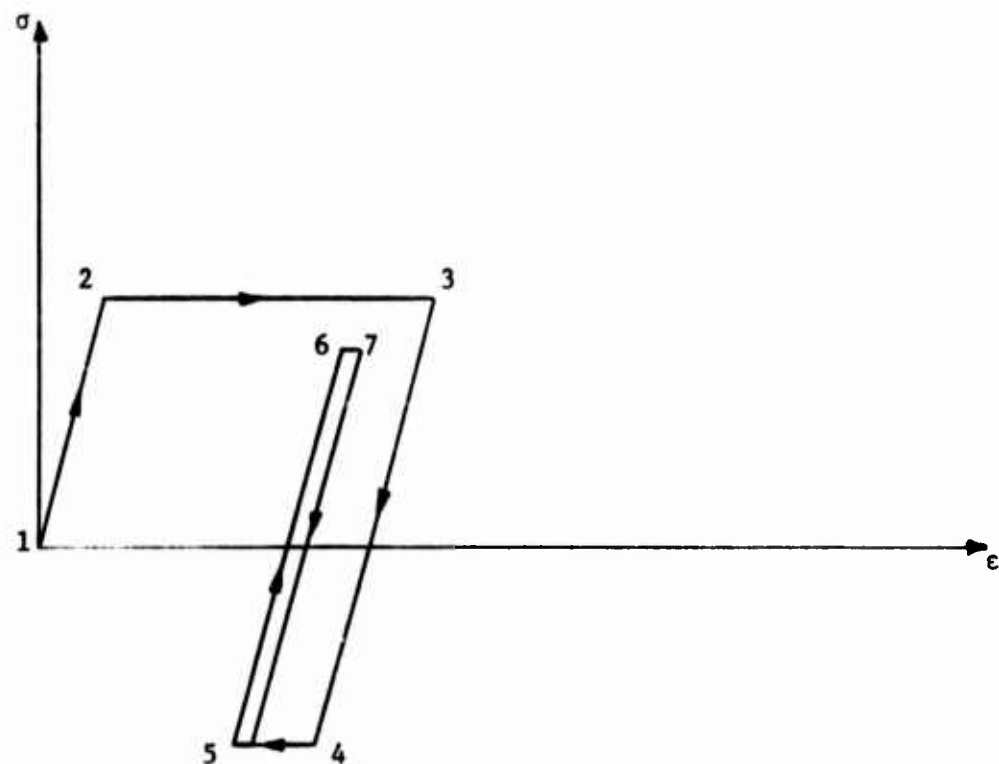


Figure 2.14. Stress-Strain Response

and

$$t_i \leq t \leq t_{i+1}, \quad x_i \leq x \leq x_{i+1} . \quad (2.9)$$

In Equations 2.4-2.8,  $x$  denotes the displacement of the mass  $m$  from the unstrained state;  $x_i$  and  $x_{i+1}$  denote the displacements at the beginning and end of the  $i^{\text{th}}$  linear response domain;  $r_i$  is the internal force acting on the mass at the beginning of the  $i^{\text{th}}$  response domain;  $E_i$ ,  $k_i$ ,  $\omega_i$  represent the slope of the stress-strain curve, the stiffness of the rod, and the natural circular frequency during the  $i^{\text{th}}$  response domain, respectively;  $A, l$  denote the area, length of the rod, respectively;  $t$  is the time measured from the application of the impulsive excitation;  $t_i$  and  $t_{i+1}$  denote the times at the beginning and end of the  $i^{\text{th}}$  response domain, respectively; and  $\tau$  denotes time measured from  $t_i$ . If the stiffness of the rod is zero during the  $i^{\text{th}}$  response domain, the displacement function is described by

$$x(\tau) = x_i + v_i \tau - \frac{1}{2} \frac{r_i}{m} \tau^2 \quad (2.10)$$

where  $v_i$  denotes the velocity of the mass  $m$  at the beginning of the  $i^{\text{th}}$  response domain.

On the basis of Equation 2.4 or 2.10, other measures of response can be obtained as follows:

$$\epsilon(\tau) = \frac{x(\tau)}{l} , \quad (2.11)$$

$\sigma(\tau)$  is determined by the strain history, Equation 2.11, and the stress-strain relation in Figure 2.12, and

$$r(\tau) = A \sigma(\tau) . \quad (2.12)$$

The exact response to a specific impulsive excitation ( $x_1 = 0$ ,  $v_1 = 10 \text{ in/sec}$ ) is depicted in Table 5 and Figure 2.14.

TABLE 5

## DYNAMIC RESPONSE OF INELASTIC ROD

DATA:  $m = 10 \text{ lb sec}^2/\text{in}$ ,  $A = .001 \text{ in}^2$ ,  $\ell = 2880 \text{ in}$ ,  $\sigma_y = 35000 \text{ psi}$

$t_1$	$\epsilon_1 / 10^{-3}$	$\sigma_1 / 10^3$	$E_1 / 10^6$	$k_1$	$\omega_1$	$x_1$	$v_1$	$r_1$
	(sec)	(psi)	(psi)	(lb/in)	(rad/sec)	(in)	(in/sec)	(lb)
1	0.000	0.000	0.000	28.800	10.000	1.000	0.000	10.000
2	0.368	1.250	36.000	0.000	0.000	0.000	3.600	9.330
3	2.960	5.448	36.000	28.800	10.000	1.000	15.689	0.000
4	5.472	3.187	-29.100	0.531	0.184	0.136	9.179	-2.119
5	6.198	2.920	-29.242	28.800	10.000	1.000	8.409	0.000
6	9.241	4.946	29.100	0.531	0.184	0.136	14.243	0.288
7	9.340	4.950	29.103	28.800	10.000	1.000	14.257	0.000
								29.103

A comparision of the response predictions produced by SINGER with the exact response is presented in Figures 2.15 and 2.16. Figure 2.15 depicts the equilibrium path of the rod, and Figure 2.16 describes the stress history of the rod. The agreement between the exact response and the response prediction of SINGER is excellent.

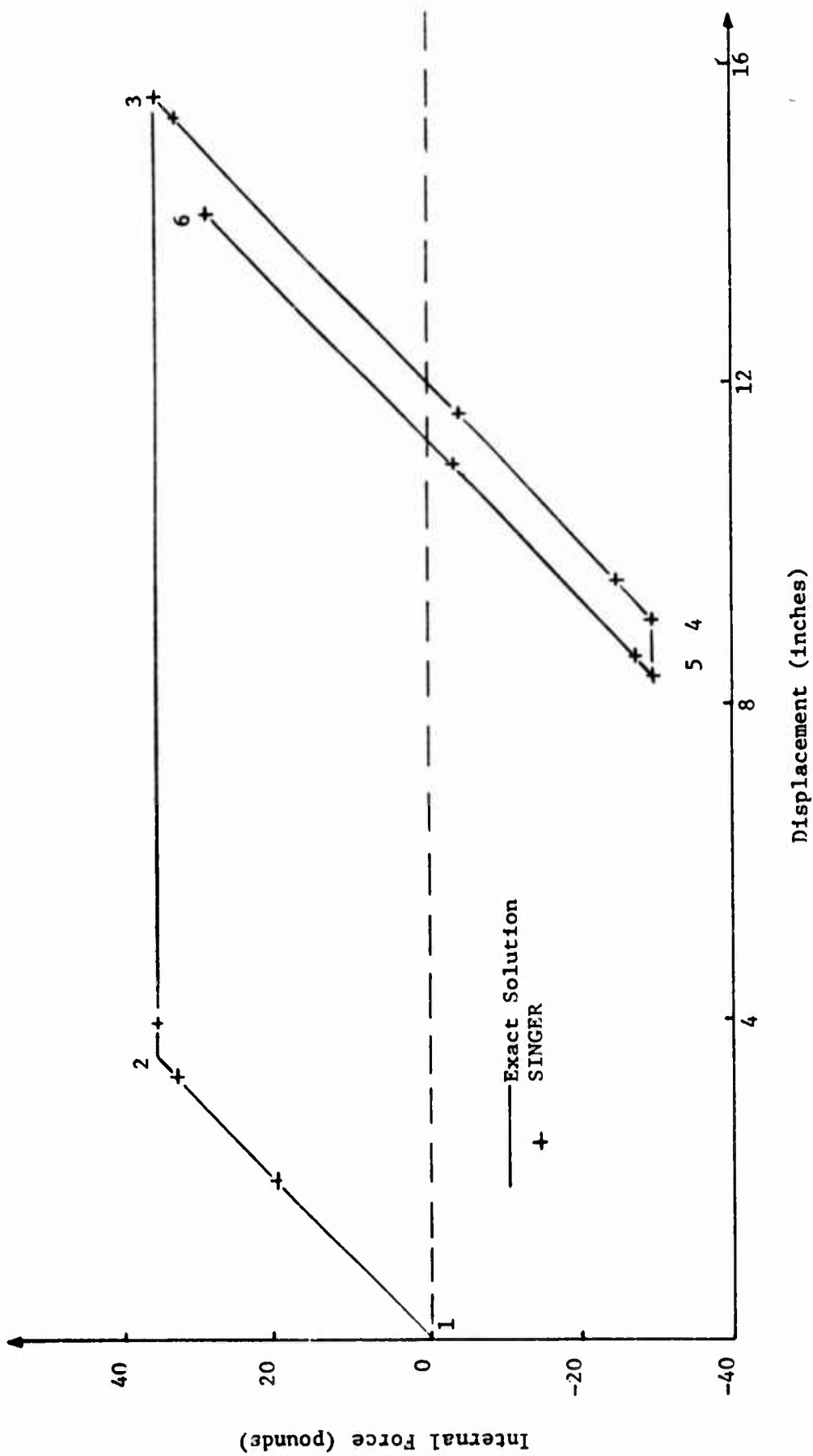


Figure 2.15. Equilibrium Path

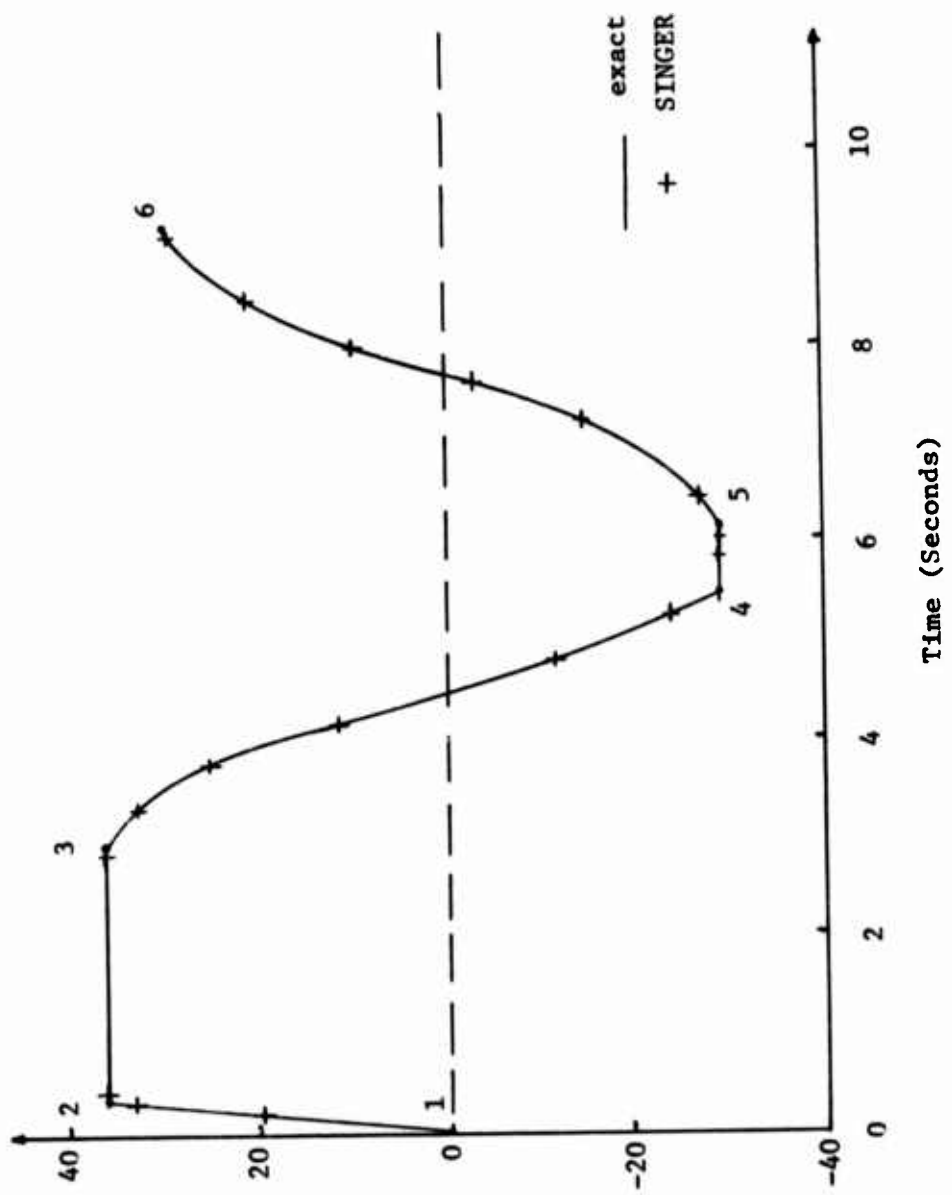


Figure 2.16. Stress History of Rod

... A VERTICAL LOAD ON THE FREE END.

OEE FI C D B O 1.00 1.0-7 15.000



## **PPI ASIIC BEAM - CANILEVERED WITH A VERTICAL LOAD ON THE FREE END, 6 ELEMENTS.**

Σ ΟΕΕ ΦΙ Κ Δ Β Ω 3.00 1.00 1.0-7 15.000

ELASTICA PROBLEM 15 FOOT - .2" X .2" BEAM SIMPLY SUPPORTED, E/L = 0.01  
 OEE FI C M B 1  
 S 1.00 36.00 1.00 1.0D-7 2.4D2

JOINT	DATA BLOCK	RRO
1	0.000	0.00
2	3.001	0.00
3	6.001	0.00
4	9.001	0.00
5	1.202	0.00
6	1.502	0.00
7	1.802	0.00
8	1.001	0.00
9	2.001	0.00
10	4.001	0.00
11	5.001	0.00
12	7.001	0.00
13	8.001	0.00
14	1.002	0.00
15	1.102	0.00
16	1.302	0.00
17	1.402	0.00
18	1.602	0.00
19	1.702	0.00
20	4.501	0.00
21	5.501	0.00
22	6.501	0.00
23	7.501	0.00
24	8.5001	0.00
25	8.7501	0.00
26	9.2501	0.00
27	9.5001	0.00
28	10.501	0.00
29	11.501	0.00

30            12.501        0.00  
31            13.501        0.00





ELASTIC RING, FIRST QUADRANT: RADIUS = 36", INTERNAL PRESSURE, 9 ELEMENTS.  
 OEE FI C D N  
 0.00 0.00 1.00 1.00 1.00-7 5.00



EDUCATIONAL FUNCTION DATA BLOCK

ELASTIC RING, FIRST QUADRANT: RADIUS = 36 $\alpha$ , INTERNAL PRESSURE, 3 ELEMENTS.

S OEE FI C 0.00 D N 1.00 OR 1.00 1.D-7 5.00

ENFORCING FUNCTION DATA BLOCK

	FUNCTION	CHARGE	EXCITATION
1	2P	OK	-2.03
2	1P	OK	2.03
2	3P	OK	-2.03
2	2P	OK	2.03
3	2P	OK	-2.03
3	4P	OK	-2.03
4	3P	OK	2.03

MASS ON THIN ROD - INITIAL VELOCITY = 10.0 INCHES/SECOND.

D      0EE      11      C      0      6      1.001      3.D-1      1.D-7      6.0D1